Journal of Power Sources 267 (2014) 610–616

Contents lists available at ScienceDirect

Journal of Power Sources

journal homepage: www.elsevier.com/locate/jpowsour

Nickel–Cobalt hydroxide microspheres electrodeposited on nickel cobaltite nanowires grown on Ni foam for high-performance pseudocapacitors

Xuefei Gong [a], J.P. Cheng [a, *], Fu Liu [a], Li Zhang [b, c], Xiaobin Zhang [a]

[a] Department of Materials Science and Engineering, State Key Laboratory of Silicon Materials, Zhejiang University, Hangzhou 310027, PR China
[b] Department of Mechanical and Automation Engineering, The Chinese University of Hong Kong, Hong Kong, PR China
[c] Shun Hing Institute of Advanced Engineering, The Chinese University of Hong Kong, Hong Kong, China

HIGHLIGHTS

- Nickel–Cobalt hydroxide microspheres were electrodeposited on $NiCo_2O_4$ nanowire arrays.
- The electrode of 10 min electrodeposition delivered a high areal capacitance of 6 F cm^{-2}.
- The synergic effect of conductive $NiCo_2O_4$ nanowires and porous hydroxides is important.

GRAPHICAL ABSTRACT

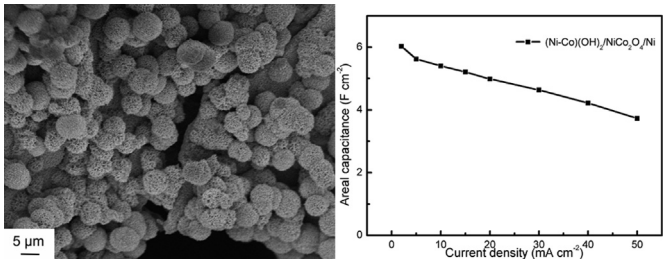

ARTICLE INFO

Article history:
Received 24 February 2014
Received in revised form
2 May 2014
Accepted 22 May 2014
Available online 2 June 2014

Keywords:
Nickel–Cobalt hydroxide
Microspheres
Electrodeposition
Ternary nickel cobaltite
Supercapacitors

ABSTRACT

Nickel–Cobalt hydroxide microspheres are electrodeposited on the films of $NiCo_2O_4$ nanowires grown on the current collector through a facile approach and the hierarchical structures are then investigated as an electrode material for high-performance supercapacitors. Owing to the superior electrical conductivity of $NiCo_2O_4$ nanowires, the porous structure of the $(Ni–Co)(OH)_2$ microspheres and the synergic effect of the multi-components, the electrode can deliver a high areal capacitance of 6 F cm^{-2} and a corresponding specific capacitance of 1132 F g^{-1} at a current density of 2 mA cm^{-2}, as well as a good rate capability (61.8% capacitance retention from 2 mA cm^{-2} to 50 mA cm^{-2}), and excellent cycling stability (90% capacitance retention after 2000 cycles). The results suggest that our research opens up the possibility for the fabrication of high-performance energy-storage devices of binder-free electrodes.

1. Introduction

Supercapacitors, also known as electrochemical capacitors, have attracted more and more attention due to their many advantages, such as high power capacity, fast charge/discharge rate and long lifespan, which can be applied in many fields including electric vehicles [1–4]. There are two types of supercapacitors based on the underlying energy storage mechanism: electrical double-layer capacitors and pseudocapacitors. In general, a pseudocapacitor electrode, usually made of transition metal oxides/hydroxides materials with multiple valence states, has excellent theoretical capacitance because of reversible Faradaic redox reactions [5–10]. For example, RuO_2 can exhibit noteworthy specific capacitance and remarkable electrochemical reversibility, while its high cost and

* Corresponding author.
E-mail address: chengjp@zju.edu.cn (J.P. Cheng).

http://dx.doi.org/10.1016/j.jpowsour.2014.05.120
0378-7753/

scarcity impede the commercial and practical applications [11]. Thus, tremendous efforts have been devoted to the synthesis of alternative electrode materials with a high-performance.

Among various metal oxides, ternary nickel cobaltite has recently aroused great interest because of some advantages such as low cost, rich sources and environmental friendliness. Moreover, it possesses much higher electrical conductivity which can facilitate a faster electron transport, and more excellent electrochemical activity resulting from simultaneous effects of nickel and cobalt ions in the Faradaic redox reactions than other metal oxides [12–15], thus it can display a wonderful electrochemical performance. For example, Xiao and co-workers successfully obtained porous $NiCo_2O_4$ of flower-like nanostructures with largely enhanced electrochemical performance (658 F g^{-1} at 1 A g^{-1} and 93.5% of specific capacitance could be retained after 1000 cycles) through a simple hydrothermal and subsequent annealing process [16]. Though $NiCo_2O_4$ shows a remarkable electrochemical performance, the experimental values of specific capacitance are still much lower than its theoretical values and not satisfactory for practical application. It is partially caused by the introduction of conductive agent and a polymer binder leading to an extra contact resistance and dead surface, thus hindering the diffusion of electrolyte. Therefore, it is desirable to grow electrode materials on current collector directly and be used as a binder-free electrode [17–19]. Thus, mesoporous $NiCo_2O_4$ nanosheets on Ni foam have been prepared, and the areal capacitance can be 3.51 F cm^{-2} at the current density of 1.8 mA cm^{-2} [14].

Meanwhile, it is necessary to seek for other materials with a high capacitance. According to results of previous literature, specific capacitances of transition metal hydroxides are usually higher than the oxides. However, metal hydroxides usually exhibit a worse cycling stability than oxides due to its low conductivity [20–28]. Therefore, to get a better electrochemical performance for a pseudocapacitor, it is highly desirable to engineer electrodes with the combination of multi-component materials, which can make use of synergistic effects from the individual constituents [29–33]. The structure of electrodes should possess large highly-accessible specific surface area to guarantee a large amount of electroactive materials to simultaneously take part in the Faradaic reactions and fast ion diffusion for supercapacitors [34]. Regarding to above considerations, it is of great significance to directly grow hierarchically multi-component materials on the current collector with highly-accessible structure as binder-free electrodes.

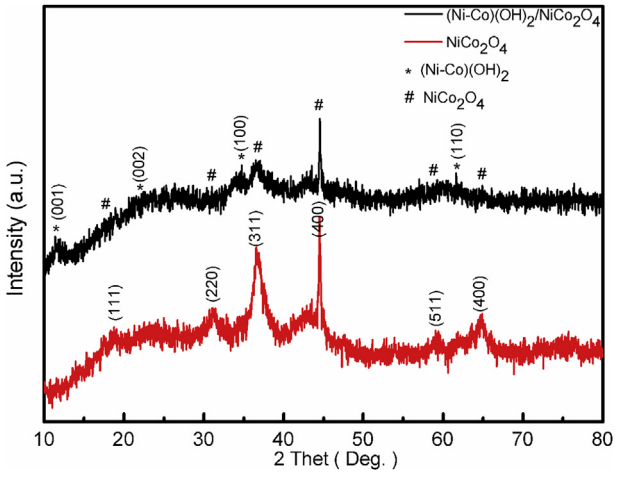

Fig. 1. XRD patterns of $NiCo_2O_4$ nanowire arrays and $(Ni–Co)(OH)_2/NiCo_2O_4$ hybrid arrays.

In this work, we developed a facile and scalable strategy to synthesize Nickel–Cobalt hydroxide microspheres electrodepositioned on $NiCo_2O_4$ nanowire arrays which were grown on Ni foam as a binder-free electrode directly. The areal capacitance of the electrode can reach 6 F cm^{-2} at a current density of 2 mA cm^{-2} and the corresponding specific capacitance is 1132 F g^{-1}. Moreover, 61.8% of its initial capacitance is maintained when the current density increases from 2 mA cm^{-2} to 50 mA cm^{-2}. The capacitance decay is only about 10% after 2000 charge–discharge cycles. The above excellent electrochemical performances indicate that the electrode can be potentially applied in practical use.

2. Experimental

2.1. Materials

All the chemicals were purchased from Aladdin, which were of analytical purity and used without any further purification.

2.2. Synthesis of $NiCo_2O_4$ nanowire arrays on Ni foam

$NiCo_2O_4$ nanowire arrays were prepared by a hydrothermal and subsequent annealing process. In a typical procedure, 1.8 mmol $Co(NO_3)_2 \cdot 6H_2O$, 0.9 mmol $Ni(NO_3)_2 \cdot 6H_2O$, and 18 mmol $CO(NH_2)_2$

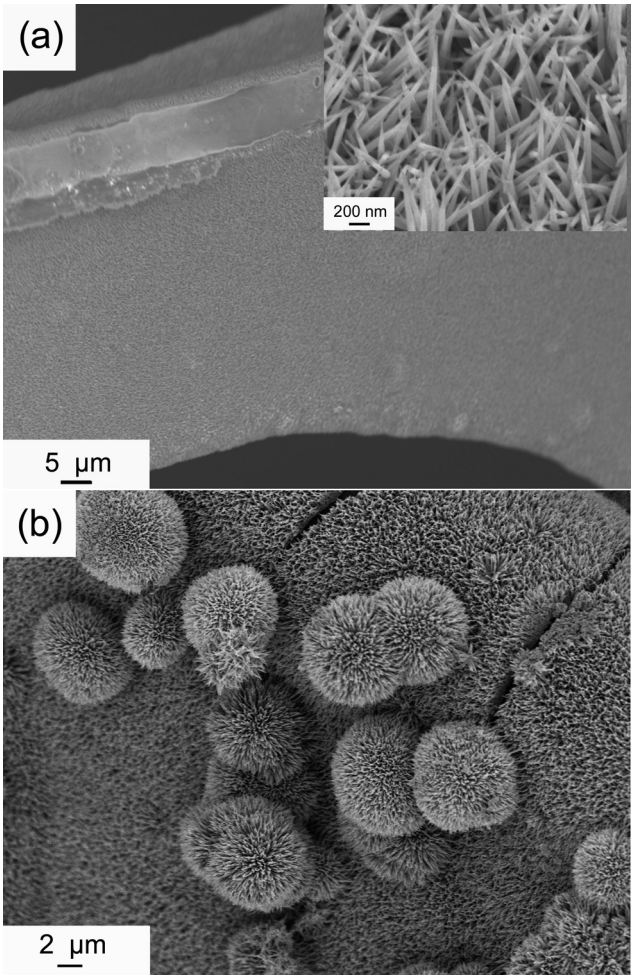

Fig. 2. (a) SEM images of the $NiCo_2O_4$ nanowire arrays grown on Ni foam. (b) SEM images of the $(Ni–Co)(OH)_2$ microspheres electrodepositioned on $NiCo_2O_4$ nanowire arrays grown on Ni foam.

were dissolved in 60 mL deionized water. After stirred for 30 min, a pink solution was obtained. Ni foam was carefully cleaned with 3 M HCl solution in an ultrasound bath for 3 min to remove the NiO layer, and then washed with deionized water. The solution and the Ni foam were then transferred into a Teflon-lined stainless-steel autoclave and maintained at 120 °C for 8 h. The as-prepared materials were then taken out, ultrasonically cleaned for 2 min in the deionized water, dried at 60 °C overnight, and finally annealed at 300 °C in N_2 atmosphere for 3 h to get $NiCo_2O_4$ nanowires. The mass loading of $NiCo_2O_4$ nanowires on Ni foam was 1.08 mg cm^{-2}.

2.3. Synthesis of (Ni–Co)$(OH)_2$ microspheres on $NiCo_2O_4$ nanowires

The growth of (Ni–Co)$(OH)_2$ microspheres on the $NiCo_2O_4$ nanowires was carried out through a simple electrodeposition method. The deposition process was performed in a standard three-electrode glass cell, in which the Ni foam (1.5 × 1.5 cm^2) covered with $NiCo_2O_4$ nanowire arrays was used as a working electrode, a saturated calomel electrode (SCE) as the reference electrode, and a Pt plate as the counter-electrode. The electrolyte was 0.1 M solution of $Co(NO_3)_2 \cdot 6H_2O$ and $Ni(NO_3)_2 \cdot 6H_2O$. The electrodeposition of Nickel–Cobalt hydroxide was performed for different periods (from 5 to 20 min) by the current static method with 50 mA cm^{-2}. The as prepared electrodes were then rinsed with deionized water and dried at 60 °C overnight. The mass load for Nickel–Cobalt hydroxide is 2.38 mg cm^{-2}, 4.24 mg cm^{-2}, 7.32 mg cm^{-2} and 11.27 mg cm^{-2} for the deposition time of 5 min, 10 min, 15 min, 20 min, respectively.

2.4. Materials characterization

The crystalline structure of as-prepared products was analyzed by powder X-ray diffraction (Shimadzu XRD-6000, CuKα. The morphological investigations of the $NiCo_2O_4$ nanowire arrays and (Ni–Co)$(OH)_2$ microspheres were carried out using a scanning electron microscope (SEM, SU-70). Nitrogen adsorption–desorption isotherms were measured at 77 K with micrometritics Coulter OMNISORP-100. The specific surface area was calculated with Brunauer–Emmett–Teller (BET) equation, and the pore size distribution was calculated from the adsorption curve by the Barrett–Joyner–Halenda (BJH) method.

2.5. Electrochemical measurements

Electrochemical measurements were performed by a three-electrode system in a solution of 2 M KOH aqueous electrolyte on a CHI660D electrochemical station. With a Pt plate as the counter-electrode and saturated calomel electrode (SCE) as the reference electrode, a Ni foam (1.5 × 1.5 cm^2) supported nanostructure was used directly as the working electrode. The cyclic voltammetry (CV) and galvanostatic charge–discharge techniques were employed to investigate the electrochemical performance of the electrodes. The electrochemical impedance spectroscopy (EIS) was obtained in the frequency range between 100 kHz and 0.01 Hz with a perturbation amplitude of 5 mV versus the open-circuit potential.

3. Results and discussion

3.1. Structure and morphology

The preparation of (Ni–Co)$(OH)_2$ microspheres involves the co-electrodeposition process. Firstly, NO_3^- is reduced on the cathodic surface accompanied by the production of OH^- ions. Then, OH^- ions combine with Ni^{2+} and Co^{2+}, resulting in the precipitation of mixed (Ni, Co) hydroxide on the working electrode surface. The process can be described in the following equations [7]:

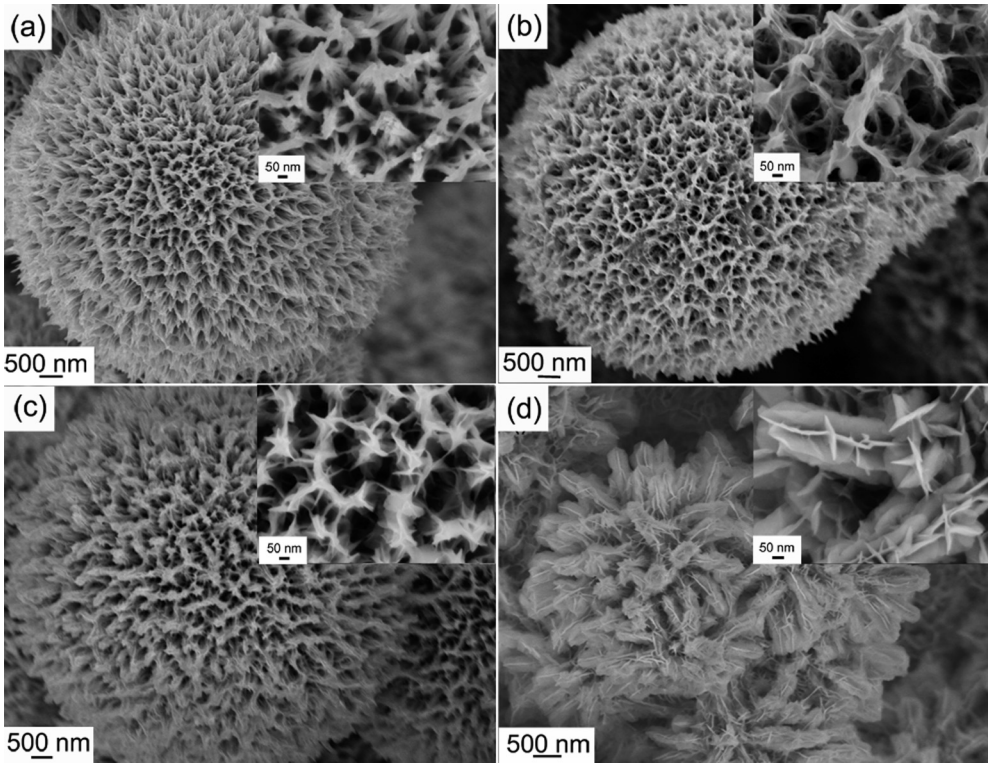

Fig. 3. Low-magnification and enlarged SEM images (the insets) of the microspheres with different electrodeposition time: (a) 5 min; (b) 10 min; (c) 15 min; (d) 20 min.

$$NO_3^- + 7H_2O + 8e^- \rightarrow NH_4^+ + 10OH^- \quad (1)$$

$$Ni^{2+} + 2OH^- \rightarrow Ni(OH)_2 \quad (2)$$

$$Co^{2+} + 2OH^- \rightarrow Co(OH)_2 \quad (3)$$

The synthesized powdered samples were obtained from the Ni foam substrate by sonication and their phase was identified by XRD. As shown in Fig. 1, the XRD pattern confirms the existence of $NiCo_2O_4$ and (Ni–Co)$(OH)_2$ phases. The diffraction peaks of $NiCo_2O_4$ nanowire arrays are observed at 18.9°, 31.1°, 36.6°, 44.6°, 59.1° and 64.9°, corresponding to the (111), (220), (311), (400), (511), and (440) planes of the $NiCo_2O_4$ phase (JCPDF 20-0781), whereas the diffraction peaks at about 11.3°, 22.6°, 34.5° and 60.7° corresponding to $Co(OH)_2$ and $Ni(OH)_2$ phases. It is difficult to differentiate the two phases because of their similarity in structure and diffraction pattern.

SEM micrographs (Fig. 2) show the morphologies of the synthesized $NiCo_2O_4$/Ni and (Ni–Co)$(OH)_2$/$NiCo_2O_4$/Ni phases. In Fig. 2a, $NiCo_2O_4$ nanowire arrays with sharp tips covered uniformly and separated apart individually on the surface of Ni foam, and such a highly open and porous structure is beneficial to the charge transport and ion diffusion. From Fig. 2b, it is apparent that the (Ni–Co)$(OH)_2$ shows a porous spherical morphology with a diameter about 5 μm. Though some microspheres are overlapped each other, the highly porous structure can still provide plenty of space for the transportation of electrolyte into the underneath part of the electrode material, which is of great importance to effectively utilize the electro-active materials and achieve excellent electrochemical performance.

Furthermore, it is noticed that the morphology of (Ni–Co)$(OH)_2$ microspheres changes with the electrodeposition time based on SEM observations as shown in Fig. 3. Obviously, as the electrodeposition time is prolonged, the building blocks of the microspheres are changed from nanoneedles (Fig. 3a) to nanosheets (Fig. 3d) due to the lateral growth of each individual, and the pore size reaches the maximum when the electrodeposition time is 10 min.

3.2. Surface area and porosity analysis

To determine the surface area and porous structure of 10 min electrodeposition (Ni–Co)$(OH)_2$/$NiCo_2O_4$ electrode, we measured the Brunauer–Emmett–Teller (BET) and nitrogen adsorption–desorption test. Fig. 4 presents the corresponding nitrogen adsorption–desorption isotherm and pore size distribution curve. Type IV isotherms with hysteresis loops can be seen from Fig. 4a, which demonstrates that the 10 min electrodeposition (Ni–Co)$(OH)_2$/$NiCo_2O_4$ arrays has a typical mesoporous structure. Meanwhile, this can be revealed from the Barrett–Joyner–Halenda (BJH) pore size distribution in Fig. 4b, which indicates the average pore size is about 7 nm. Nitrogen adsorption–desorption results show that the arrays had a BET surface area of 29 $m^2\ g^{-1}$ with a pore volume of 0.053 $cm^3\ g^{-1}$. The mesoporous structure can provide efficient transport for electrons and ions, making a significant contribution to a high electrochemical capacity.

3.3. Electrochemical properties

Galvanostatic discharge measurements of the electrodes with various electrodeposition time at the current density of 2 mA cm^{-2} are shown in Fig. 5a, and the calculated mass specific capacitances and areal capacitances are shown in Fig. 5b and c, respectively. The results indicate that the electrode with 20 min electrodeposition shows the highest areal capacitance of 12 F cm^{-2}, while the

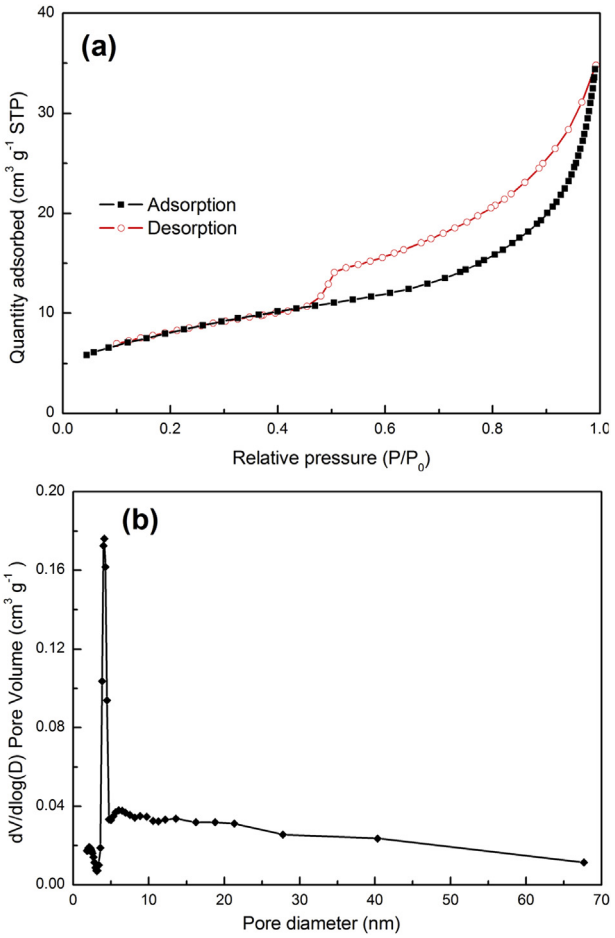

Fig. 4. Nitrogen adsorption–desorption isotherms (a) and the pore size distribution plot (b) of 10 min electrodeposition (Ni–Co)$(OH)_2$ on $NiCo_2O_4$ arrays.

electrode with 10 min electrodeposition exhibits the highest specific capacitance, indicating the better utilization of the electroactive materials. The rate capabilities, a key factor for evaluating the power applications of the supercapacitors, were also measured with the current density from 2 to 50 mA cm^{-2} (Fig. 5c). It can be seen that the areal capacitance retention is 51.7%, 61.8%, 46.4% and 35.1% for the electrodes with the electrodeposition time of 5, 10, 15 and 20 min, respectively. Moreover, the cycling performances were evaluated by the repeated charging/discharging measurement at a constant current densities of 20 mA cm^{-2}. As showed in Fig. 5d, the electrodes for 5, 10, 15 and 20 min electrodeposition displayed different cycling stability, with about 93%, 90%, 83%, 77% capacitance retention after 2000 cycles, respectively, indicating that the high proportion of (Ni–Co)$(OH)_2$ material is detrimental to the cycling stability due to its low conductivity. Overall, the electrode of 10 min electrodeposition exhibited better comprehensive electrochemical behavior.

To evaluate the supercapacitor applications and highlight the merits of the unique architecture of the 10 min deposition electrode, the electrochemical properties were further investigated. Fig. 6a shows the CV curves of $NiCo_2O_4$/Ni and (Ni–Co)$(OH)_2$/$NiCo_2O_4$/Ni electrodes at a scan rate of 2 mV s^{-1} in the potential range of −0.2 V to 0.6 V. Apparently, a pair of redox peaks at about 0.2 V and 0.36 V is observed for the electrode containing $NiCo_2O_4$ nanowires, which correspond to the reversible reactions of Co^{3+}/Co^{4+} and Ni^{2+}/Ni^{3+} transitions associated with anions OH^- [35,36]. Remarkably, the same redox peaks can be still found for the

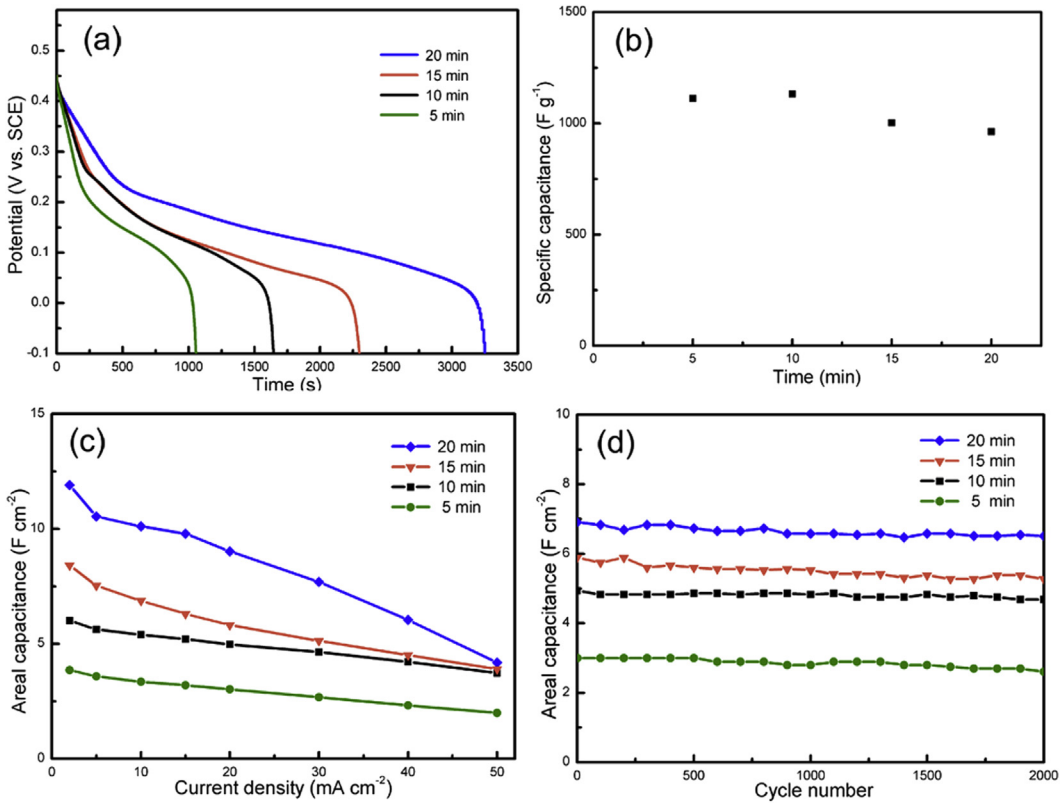

Fig. 5. (a) Discharge curves of the electrodes with different electrodeposition time at the current density of 2 mA cm^{-2}. (b) Specific capacitance with different electrodeposition time. (c) Areal capacitance with different electrodeposition time at various current densities. (d) Cycling performance with different electrodeposition time at the current density of 20 mA cm^{-2}.

(Ni–Co)$(OH)_2$/$NiCo_2O_4$ electrode, indicating the efficient utilization of the embedding $NiCo_2O_4$ nanowire arrays. Moreover, we can also observe one more pair of redox peaks at about 0.05 V and 0.3 V, due to the lower redox potential of M–OH/M–O–OH (M represents Ni and Co ions) [37]. Further, the larger of the area integrated within the current-potential curves indicates the higher of electrochemical reaction activity and capacitance. Obviously, (Ni–Co)$(OH)_2$/$NiCo_2O_4$/Ni electrode exhibits a higher capacitance than $NiCo_2O_4$/Ni, which can also be verified by the following galvanostatic charge–discharge measurements. Fig. 6b shows the galvanostatic charge–discharge curves of $NiCo_2O_4$/Ni and (Ni–Co)$(OH)_2$/$NiCo_2O_4$/Ni electrodes within the voltage range between −0.1 and 0.45 V at a current density of 2 mA cm^{-2}. Areal capacitances of 6 F cm^{-2} and 0.6 F cm^{-2} can be achieved at the current density of 2 mA cm^{-2} for the (Ni–Co)$(OH)_2$/$NiCo_2O_4$/Ni and $NiCo_2O_4$/Ni electrodes, respectively, which indicates that the (Ni–Co)$(OH)_2$ porous microspheres make a great contribution to the overall areal capacitance. The non-linear curve in shape again corroborates the pseudocapacitance behavior. At the current density of 2 mA cm^{-2}, the calculated specific capacitance of 1132 F g^{-1} is much higher compared with previously reported directly-grown pseudocapacitors, such as Co_3O_4@NiO core–shell nanowires structure electrode (2.56 F cm^{-2}, 857 F g^{-1}) [38].

To further examine the electrochemical performances of the 10 min deposited (Ni–Co)$(OH)_2$/$NiCo_2O_4$/Ni electrode, we performed the CV tests at different scan rates of 2, 5 and 10 mV s^{-1} in the potential range of −0.2 to 0.6 V. Fig. 6c reveals that the position of the cathodic peak shifts from 0.3 to 0.4 V, and the anodic peak from 0.05 to 0.1 V. This is attributed to a relatively low resistance and good contact between the electrolyte and the electroactive materials. However, with the increase of the scan rate, only one pair of redox peaks can be observed, because the high scan rate inhibits ions from penetrating into the inner nanostructures of the electrode material and the utilization of the active material is decreased.

Moreover, electrochemical impedance spectroscopies (EIS) analysis was measured in order to well understand the remarkable electrochemical behavior. As shown in Fig. 6d, in low frequency area, the electrode has an ideal straight line along the imaginary axis, indicating a low Warburg impedance (W) and thus performing low electrolyte diffusion resistance. Further, in the high frequency area, the electrode exhibits bulk solution resistance of 0.62 Ω and charge-transfer resistance of 0.21 Ω, which can be estimated from the intersection and semicircle of the curve at real axis, thus the 10 min electrodeposed (Ni–Co)$(OH)_2$/$NiCo_2O_4$/Ni electrode has excellent capacitive behavior.

The above electrochemical measurements suggest that the directly-grown binder-free (Ni–Co)$(OH)_2$/$NiCo_2O_4$/Ni hybrid electrode delivers excellent capacitive properties and they are good candidates for practical use [39]. The reasons for the remarkable electrochemical performance are as follows. (1) $NiCo_2O_4$ nanowires can not only act as the backbone to support and the reservoir for electrolyte, but also ensure the electrons transfer easily to participate in the redox reactions and make full utilization of the electroactive materials due to the high electrical conductivity. The $NiCo_2O_4$ nanowires can also make partial contribution to the electrochemical performance. (2) The porous structure of the electrode effectively enhances the surface area and ensures a fast ion transport. (3) The electrodes made of multi-component materials can make use of synergistic effects from the individual constituents. (4) The as-prepared electrodes can be directly used, avoiding the use of polymer binders and conductive additives.

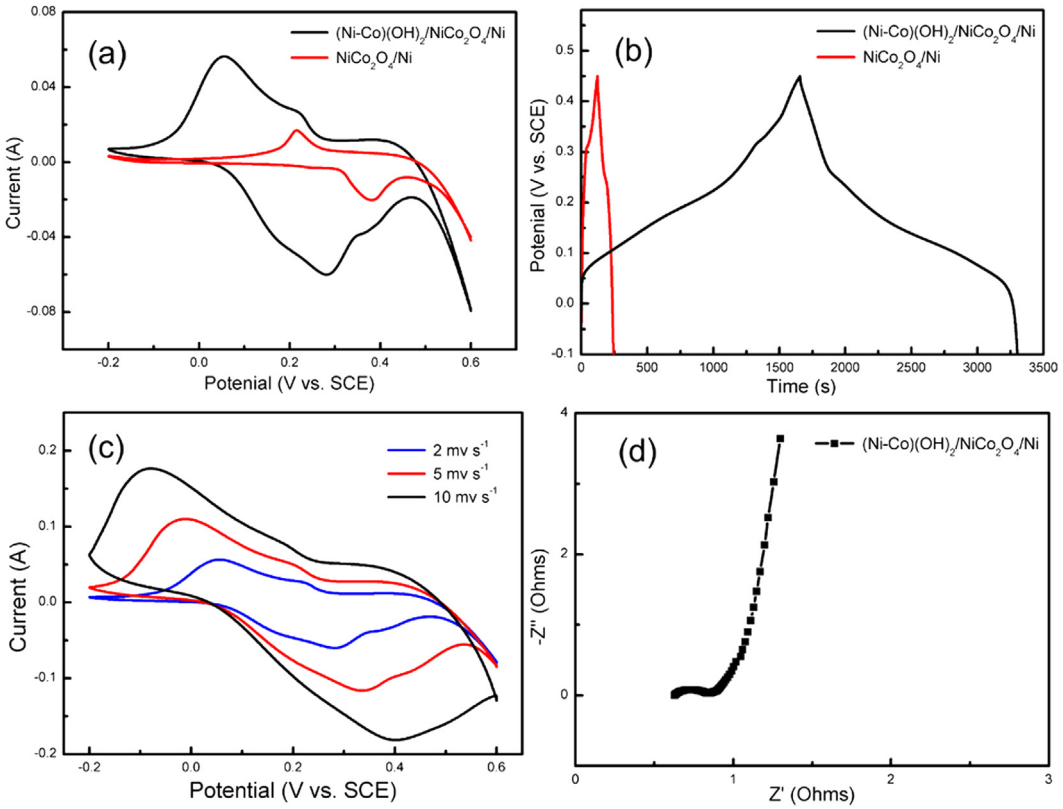

Fig. 6. (a) Cyclic voltammograms of $NiCo_2O_4$/Ni and 10 min electrodeposition (Ni–Co)$(OH)_2$/$NiCo_2O_4$/Ni electrodes in 2 M KOH aqueous electrolyte at a scan rate of 2 mV s^{-1}. (b) Charge–discharge curves of $NiCo_2O_4$/Ni and 10 min electrodeposition (Ni–Co)$(OH)_2$/$NiCo_2O_4$/Ni electrodes at the current density of 2 mA cm^{-2}. (c) Cyclic voltammograms of 10 min electrodeposition (Ni–Co)$(OH)_2$/$NiCo_2O_4$/Ni electrode at different scan rates. (d) EIS Nyquist plots of 10 min electrodeposition (Ni–Co)$(OH)_2$/$NiCo_2O_4$/Ni electrode.

4. Conclusions

In summary, a binder-free porous structure electrode with remarkable electrochemical performance has been successfully developed through a facile and scalable strategy. The as-prepared hybrid electrode delivers excellent performance of 6 F cm^{-2} at the current density of 2 mA cm^{-2} and the corresponding specific capacitance is 1132 F g^{-1}. The high conductivity, porous structure and synergic effect play significant roles to the excellent electrochemical performances. This work opens up the possibility for the fabrication of high-performance energy-storage devices with binder-free electrodes directly-grown on current collectors.

Acknowledgments

This work was supported by Zhejiang Provincial Natural Science Foundation of China (No. LY13E020002), Experimental Research Project of Zhejiang University, and the Project No. RNE-p4-13 of the Shun Hing Institute of Advanced Engineering, The Chinese University of Hong Kong.

Appendix A. Supplementary data

Supplementary data related to this article can be found at http://dx.doi.org/10.1016/j.jpowsour.2014.05.120.

References

[1] M.S. Dresselhaus, I.L. Thomas, Nature 414 (2001) 332–337.
[2] P. Simon, Y. Gogotsi, Nat. Mater. 7 (2008) 845–854.
[3] J.R. Miller, P. Simon, Science 321 (2008) 651–652.
[4] P.J. Hall, M. Mirzaeian, S.I. Fletcher, F.B. Sillars, A.J.R. Rennie, G.O. Shitta-Bey, G. Wilson, A. Crudenb, R. Carter, Energy Environ. Sci. 3 (2010) 1238–1251.
[5] Z. Chen, V. Augustyn, J. Wen, Y.W. Zhang, M.Q. Shen, B. Dunn, Y.F. Lu, Adv. Mater. 23 (2011) 791–795.
[6] M. Kundu, L.F. Liu, J. Power Sources 243 (2013) 676–681.
[7] C.Z. Yuan, J.Y. Li, L.R. Hou, X.G. Zhang, L.F. Shen, X.W. Lou, Adv. Funct. Mater. 22 (2012) 4592–4597.
[8] B. Zhang, Y.B. Zhang, Z.Z. Miao, T.X. Wu, Z.D. Zhang, X.G. Yang, J. Power Sources 248 (2014) 289–295.
[9] D.D. Han, P.C. Xu, X.Y. Jing, J. Wang, P.X. Yang, Q.H. Shen, J.Y. Liu, D.L. Song, Z. Gao, M.L. Zhang, J. Power Sources 235 (2013) 45–53.
[10] M. Hakamada, A. Moriguchi, M. Mabuchi, J. Power Sources 245 (2014) 324–330.
[11] A. Devadas, S. Baranton, T.W. Napporn, C. Coutanceau, J. Power Sources 196 (2011) 4044–4053.
[12] T.-Y. Wei, C.-H. Chen, H.-C. Chien, S.-Y. Lu, C.-C. Hu, Adv. Mater. 22 (2010) 347–351.
[13] H.L. Wang, Q.M. Gao, L. Jiang, Small 7 (2011) 2454–2459.
[14] G.Q. Zhang, X.W. Lou, Adv. Mater. 25 (2013) 976–979.
[15] H. Jiang, J. Ma, C.Z. Li, Chem. Commun. 48 (2012) 4465–4467.
[16] J.W. Xiao, S.H. Yang, RSC Adv. 1 (2011) 588–595.
[17] F.Z. Deng, L. Yu, G. Cheng, T. Lin, M. Sun, F. Ye, Y.F. Li, J. Power Sources 251 (2014) 202–207.
[18] X.Y. Liu, Y.Q. Zhang, X.H. Xia, S.J. Shi, Y. Lu, X.L. Wang, C.D. Gu, J.P. Tu, J. Power Sources 239 (2013) 157–163.
[19] H.C. Chen, J.J. Jiang, L. Zhang, T. Qi, D.D. Xia, H.Z. Wan, J. Power Sources 248 (2014) 28–36.
[20] V. Gupta, S. Gupta, N. Miurab, J. Power Sources 189 (2009) 1292–1295.
[21] C.-C. Hu, C.-T. Hsu, K.-H. Chang, H. Yu Hsu, J. Power Sources 238 (2013) 180–189.
[22] X. Sun, G.K. Wang, H.T. Sun, F.Y. Lu, M.P. Yu, J. Lian, J. Power Sources 238 (2013) 150–156.
[23] C.-W. Kung, H.-W. Chen, C.-Y. Lin, R. Vittal, K.-C. Ho, J. Power Sources 214 (2012) 91–99.
[24] G. Chen, S.S. Liawa, B.S. Li, Y. Xua, M. Dunwell, S.G. Deng, H.Y. Fan, H.M. Luo, J. Power Sources 251 (2014) 338–343.
[25] Z.H. Yang, F. F Xu, W.X. Zhang, Z.S. Mei, B. Pei, X. Zhu, J. Power Sources 246 (2014) 24–31.
[26] R. Tummala, R.K. Guduru, P.S. Mohanty, J. Power Sources 209 (2012) 44–51.
[27] W.F. Zhang, C. Ma, J.H. Fang, J.P. Cheng, X.B. Zhang, S.R. Dong, L. Zhang, RSC Adv. 3 (2013) 2483–2490.

[28] J.H. Fang, M. Li, Q.Q. Li, W.F. Zhang, Q.L. Shou, F. Liu, X.B. Zhang, J.P. Cheng, Electrochim. Acta 85 (2012) 248–255.
[29] Z.Y. Lu, Q. Yang, W. Zhu, Z. Chang, J.F. Liu, X.M. Sun, D.G. Evans, X. Duan, Nano Res. 5 (2012) 369–378.
[30] Q. Li, Z.L. Wang, G.R. Li, R. Guo, L.X. Ding, Y.X. Tong, Nano Lett. 12 (2012) 3803–3807.
[31] J.-H. Kim, K. Zhu, Y.F. Yan, C.L. Perkins, A.J. Frank, Nano Lett. 10 (2010) 4099–4104.
[32] L.-Q. Mai, F. Yang, Y.-L. Zhao, X. Xu, L. Xu, Y.-Z. Luo, Nat. Commun. 2 (2011) 381.
[33] X.H. Xia, J.P. Tu, Y.Q. Zhang, Y.J. Mai, X.L. Wang, C.D. Gu, X.B. Zhao, J. Phys. Chem. C 115 (2011) 22662–22668.
[34] C.Z. Yuan, B. Gao, L.F. Shen, S.D. Yang, L. Hao, X.J. Lu, F. Zhang, L.J. Zhang, X.G. Zhang, Nanoscale 3 (2011) 529–545.
[35] Y.G. Li, P. Hasin, Y.Y. Wu, Adv. Mater. 22 (2010) 1926–1929.
[36] X. Chen, J.P. Cheng, Q.L. Sou, F. Liu, X.B. Zhang, CrystEngComm 14 (2012) 1271–1276.
[37] F. Zhang, C.Z. Yuan, X.J. Lu, L.J. Zhang, Q. Che, X.G. Zhang, J. Power Sources 203 (2012) 250–256.
[38] X.H. Xia, J.P. Tu, Y.Q. Zhang, X.L. Wang, C.D. Gu, X.-B. Zhao, H.J. Fan, ACS Nano 6 (2012) 5531–5538.
[39] J.P. Cheng, J.H. Fang, M. Li, W.F. Zhang, F. Liu, X.B. Zhang, Electrochim. Acta 114 (2013) 68–75.